Research Article Vol. 14, No. 11 / 1 Nov 2023 / Biomedical Optics Express 5851
Biomedical Optics EXPRESS

OCT-angiography based artificial intelligence-inferred fluorescein angiography for leakage detection in retina [Invited]

TOSHINORI MURATA,[1] TAKAO HIRANO,[1] HIDEAKI MIZOBE,[2] AND SHUHEI TOBA[2]

[1]*Department of Ophthalmology, School of Medicine, Shinshu University, 3-1-1 Asahi Matsumoto, Nagano, 390-8621, Japan*
[2]*Canon Inc. 30-2, Shimomaruko 3-chome, Ohta-ku, Tokyo 146-8501, Japan*

Abstract: Optical coherence tomography angiography (OCTA) covers most functions of fluorescein angiography (FA) when imaging the retina but lacks the ability to depict vascular leakage. Based on OCTA, we developed artificial intelligence-inferred-FA (AI-FA) to delineate leakage in eyes with diabetic retinopathy (DR). Training data of 19,648 still FA images were prepared from FA-photo and videos of 43 DR eyes. AI-FA images were generated using a convolutional neural network. AI-FA images achieved a structural similarity index of 0.91 with corresponding real FA images in DR. The AI-FA generated from OCTA correctly depicted vascular occlusion and associated leakage with enough quality, enabling precise DR diagnosis and treatment planning. A combination of OCT, OCTA, and AI-FA yields more information than real FA with reduced acquisition time without risk of allergic reactions.

1. Introduction

The golden standard examination tool to delineate retinal vessels and their pathologies has been fluorescein angiography (FA), which requires contrast dye injection. Recently, optical coherence tomography-angiography (OCT-A) [1,2] has gained popularity due to its ability to delineate retinal vessels without the use of contrast dye, thus eliminating concerns about allergic complications including anaphylactic shock completely. OCT-A can depict retinal vessels to the capillary level utilizing dynamics of red blood cells, their occlusions, and neovascularization [3,4]. However, one of the reasons why OCT-A has not entirely replaced conventional FA yet is because it is difficult, if not impossible, for OCT-A to detect vascular leakage [3,5]. This limitation is particularly significant in certain diseases, such as diabetic macular edema and uveitis, where vascular leakage is crucial in their pathogenesis.

Among these conditions, the most prevalent is diabetic macular edema, which occurs at all stages of diabetic retinopathy, from non-proliferative to proliferative stages. It is a leading cause of legal blindness or severe visual impairment with vision worse than 20/200 [6]. Early intervention can restore vision, but persistent macular edema can lead to permanent visual impairment due to the destruction of photoreceptors and other neural retinal structures [7]. Macular edema is the accumulation of plasma components leaked from retinal blood vessels into the neural retina. The authors reported that vascular endothelial growth factor (VEGF) is the causative substance for the leakage in diabetic macular edema by inducing the breakdown of the blood-retinal barrier of the retinal vessels in 1995 [8]. Currently, the most effective treatment to stop leakage and absorb macular edema is the intravitreal injection of anti-VEGF drugs. However, this treatment requires approximately 7 to 9 injections per year, posing a significant socio-economic burden to the patient and making treatment adherence of diabetic macular edema patients challenging [9]. In Japan, based on prescription-based research, the average annual number of injections for diabetic macular edema patients remains around 2 injections [10].

#506467 https://doi.org/10.1364/BOE.506467
Journal © 2023 Received 19 Sep 2023; revised 12 Oct 2023; accepted 12 Oct 2023; published 18 Oct 2023

Biomedical Optics EXPRESS

To reduce the economic burden on patients by minimizing the number of anti-VEGF drug injections, focal/direct laser of leaking microaneurysms is the most reliable adjunct treatment when they are located more than 500 μm away from the fovea, where we can deliver focal/direct laser treatment. The focal/direct laser is effective, especially when leaking microaneurysms are located in the middle of the circinate retinopathy and are photo-coagulable [11–13]. Thus, in determining the treatment approach for macular edema, identifying the site of vascular leakage or the leaking microaneurysms is crucial [14–16]. However, as mentioned earlier, OCT-A cannot depict leakage, and its ability to visualize microaneurysms is also limited partly because they are difficult to identify without associated leakage. As mentioned above, OCT-A relies on the dynamics of red blood cells to depict blood vessels instead of contrast dyes [17,18].

To compensate for this limitation of OCT-A caused by the inability to detect leakage, a method has been considered to infer the leakage area by overlaying images of retinal thickening due to edema resulting from leakage onto OCT-A images among diabetes or uveitis patients [19]. Macular edema can arise from various retinal conditions, including diabetic retinopathy, branch retinal vein occlusion (BRVO), and uveitis with retinal vasculitis. However, overlaying the macular thickness map and OCT-A is time-consuming as a daily clinical practice. Moreover, retinal thickening can occur not only by increased leakage but also by decreased pump function of the retinal pigment epithelium as well, so it may not accurately reflect the leakage of retinal vessels [20].

In routine clinical practice, to make OCT-A a valuable tool at the same level as conventional FA in treating macular edema from various disease entities, we considered that it is necessary to develop an algorithm based on deep learning using AI to delineate leakage on conventional OCT-A images. Thus, we performed a study to make an AI-assisted OCT-A, which delineates vascular leakage without contrast dye injection. We report AI-inferred-FA that is based on OCT-A, which can depict leakage using deep learning with a Convolutional Neural Network (CNN).

2. Materials and methods

2.1. Dataset

The dataset used in this study was obtained from the patients with diabetic retinopathy who visited the outpatient clinic of the Department of Ophthalmology at Shinshu University, Japan, between 2019 and 2022. The dataset was used to establish a CNN algorithm to generate AI-inferred-FA images from the corresponding OCT-A images. Forty-three wide-field OCT-A (23×20 mm) images from 43 eyes with diabetic retinopathy were obtained, and corresponding FA images were also obtained on the same day. A total of 19,648 still FA images were prepared as the training data for the CNN algorithm. These wide-field OCT-A images (23 mm x 20 mm) were obtained using Xephilio OCT-S1 (Canon, Tokyo, Japan) from 43 eyes of 26 patients with diabetic retinopathy. FA images and the fluorescein videos of the early phase were also obtained from each eye using Heidelberg Spectralis (Heidelberg Engineering, Heidelberg, Germany) on the same day as OCT-A images were obtained. The training data of the CNN algorithm consisted of the still FA images obtained during routine examinations of the eyes mentioned above with diabetic macular edema, and the still FA video-frame images generated from FA videos taken from the arterial phase that usually continued about 30 to 45 seconds. To verify whether the CNN algorithm, trained on FA images of diabetic retinopathy, can be generalized for other diseases causing macular edema, AI-inferred-FA images were also generated and compared with real FA images in four eyes with BRVO, another vascular occlusive condition where anti-VEGF drugs are useful in its treatment, and in three eyes with Bechet disease, which exhibit inflammatory vascular leakage in the retina. The current study was performed in accordance with the tenets of the Declaration of Helsinki and was approved by the institutional review board of Shinshu University

Biomedical Optics EXPRESS

(clinical research approval number 5674). Informed consent from patients was obtained by the opt-out method.

2.2. Cleansing of FA images

Real FA images and wide-field OCT-A were obtained on the same day from each eye. AI-inferred FA was generated based on the OCT-A by CNN deep learning algorithm using real FA as training data. The image quality of training data was crucial to ensure the accuracy of vascular leakage detection by AI-inferred-FA. Consequently, the following categories of FA images were excluded from the training dataset of the current CNN algorithm generation.

1. FA images with noticeable noise.
2. FA images with improper focus during acquisition, resulting in unclear visualization of vascular structures.
3. Images showing retinal photocoagulation scars, as they are not depicted in OCT-A images and were deemed impossible to infer from OCT-A images to AI-inferred-FA images.
4. FA images in which only partial images are available, with prominent differences between bright and dark regions.

2.3. Alignment of OCT-A and real FA images

Tavakkoli et al. [21] reported an FA-like image generation based on a fundus photograph without apparent pathological conditions using deep learning CNN-generative adversarial networks (GAN) algorithm. In their study, training on unaligned images hampered the synthesizing FA like images with vessels distorted or missing. They reported that to address such problems, there was a need to align the FA images with their fundus counterparts prior to CNN training.

In the current study, since original pairs of OCT-A and real FA images were naturally unaligned, image modification on the FA image side was performed by a non-rigid registration using the large deformation diffeomorphic metric mapping (LDDMM) method [22] so that the pixel coordinates of anatomical structures matched between two images, an OCT-A image and a FA image, acquired from the same eye on the same day.

2.4. Preprocessing of images

The dataset used in the current CNN algorithm to generate AI-inferred-FA images from the corresponding OCT-A images consisted of 43 wide-field OCT-A (23×20 mm) images and the corresponding 19,648 still FA images in total used as training data. The 19,648 still FA images used as training data consisted of 7,198 images that were actually obtained for routine examinations still FA frame images were obtained from 30-45 second videos, comprising 5,666 images of 30 degrees FA images and 1,532 images of 55 degrees FA images.

In addition, for the purpose of creating a continuous 300-second video of AI-inferred FA based on an OCT-A image, the 19,648 images include additional FA images generated by the interpolation method for the time period when the actual captured FA image did not exist, corresponding to the time when the opposite eye was being photographed, or during the recess between the early and late phases of the images acquisition.

2.5. AI-inferred-FA image generation by CNN

In the training process of the CNN algorithm to generate AI-inferred-FA, a set of 30 OCT-A images (from 30 eyes) along with their corresponding FA images for each eye was utilized as the training dataset, totaling 19,648 still FA images. Additionally, a separate set of 8 OCT-A images

Biomedical Optics EXPRESS

(from 8 eyes) was used for validation, and finally a distinct set of 5 images (from 5 eyes) was employed for evaluating the performance of this CNN algorithm.

The CNN algorithm was developed through a process of training the CNN while confirming the increase in structural similarity (SSIM) between AI-inferred FA and the corresponding training FA data. This was carried out utilizing in the set of 30 OCT-A images prepared for the training process.

The training of the CNN algorithm was repeated until the SSIM between the AI-inferred FA images and the corresponding real FA images, calculated across 8 validation OCT-A images, reached a point where it stopped increasing and commenced decreasing. Finally, the SSIMs of the AI-inferred FA image and the corresponding FA images were computed using the five OCT-A images saved as evaluation data.

A CNN-based U-Net [23,24] encoder-decoder architecture was designed as an image generation algorithm that outputs an AI-inferred FA image of the desired specific imaging time based on an OCT-A image obtained on the same day, as shown in Fig. 1.

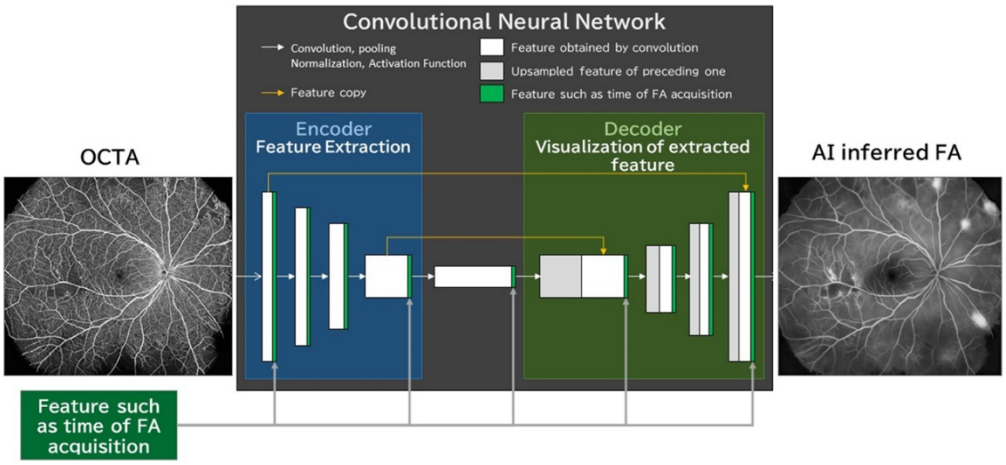

Fig. 1. Feature extraction from OCT-A and visualization of the extracted features for creating AI-inferred-FA images.

The encoder consists of processing layers such as convolution layers, pooling layers, batch normalization layers, and activation functions. The decoder reconstructs features extracted from the encoder using upsampling to generate an FA-like image closely resembling a real FA image, which is an AI-inferred FA image.

The specific input data to this CNN model algorithm is the tensors based on the pixel values of OCT-A image data and a scalar value of image acquisition time (millisecond). The scalar value indicating the image acquisition time is designed to be input to the AI-inferred FA generation CNN algorithm by concatenating it with the feature tensors extracted in the CNN algorithm described above. The model training settings were as follows. The optimizer used for training was SGD [25], and the learning rate was set to 1.8896. This specific learning rate was determined through hyperparameter tuning. The training process also employed a Cyclic Scheduler [26] for adjusting the learning rate.

The loss function utilized during training was based on SSIM [27], and the model architecture was designed around a network based on U-Net [23]. In each mini-batch, 16 data points were processed. For the training environment, PyTorch library was used to implement the CNN. The training was carried out on 4 GPUs, specifically the NVIDIA GeForce RTX 3090.

Biomedical Optics EXPRESS

2.6. Application of AI-inferred FA for detecting leakage in other retinal diseases

The current CNN algorithm to delineate retinal vascular leakage was developed using real FA of diabetic retinopathy as training data. To broaden its application, OCT-A images of branch retinal vein occlusion (BRVO), which is the second most common retinal vascular occlusive disease [28], were also investigated if AI-inferred-FA successfully delineates leakage. We also conducted further investigation to determine the effectiveness of this CNN algorithm in detecting retinal vascular leakage caused by inflammation. Retinal vasculitis in Behcet's disease is known to display leakage in unique fern-like patterns. We investigated whether AI-inferred-FA can reproduce such fern-like leakage patterns based on OCT-A images.

2.7. FA image generation at various time points and FA video generation

In real FA, according to the elapsed time after contrast dye injection, the extent of leakage continues to increase in the early phase, and the FA images undergo significant changes accordingly. Therefore, it was important to incorporate the element of time progression during the training of the current CNN algorithm for AI-inferred-FA.

To achieve this objective, we assembled a dataset of 150 still FA images, each captured at distinct time intervals ranging from 0 to 300 seconds after the injection of the fluorescein contrast dye. However, during the examination of the other eye, no still FA images could be obtained, resulting in missing data points, as shown in Fig. 2.

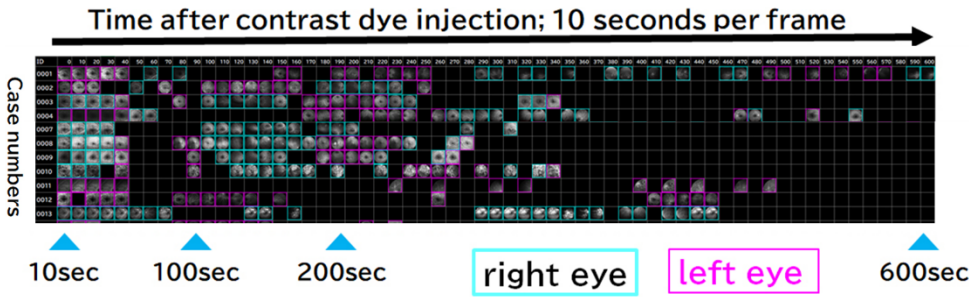

Fig. 2. The dataset comprises FA images organized chronologically for each individual case.

To address these gaps, interpolation techniques were employed to fill in the missing time intervals. Utilizing still AI-inferred FA images along with elapsed time information, we also generated AI-inferred-FA videos. The AI-inferred-FA videos are 15-second movies generated by concatenating 150 still AI-inferred-FA images corresponding to 300 seconds of real time.

3. Results

3.1. AI-inferred FA based on OCT-A in diabetic retinopathy

OCT-A delineates defined retinal vessel images to capillary levels in diabetic retinopathy, and provides information on capillary occlusion and neovascularization, but not vascular leakage as shown in Fig. 3(a). Conventional FA of the same eye delineates non-perfusion areas and associated vascular leakage, as shown in Fig. 3(b). The AI-inferred-FA image clearly depicted non-perfusion areas and associated vascular leakage in a closely similar manner to the conventional FA, as shown in Fig. 3(c). The areas with leakage correctly corresponded to those of macular edema (thickened area) depicted as red/white-colored lesions with an OCT thickness map, as shown in Fig. 3(d).

Biomedical Optics EXPRESS

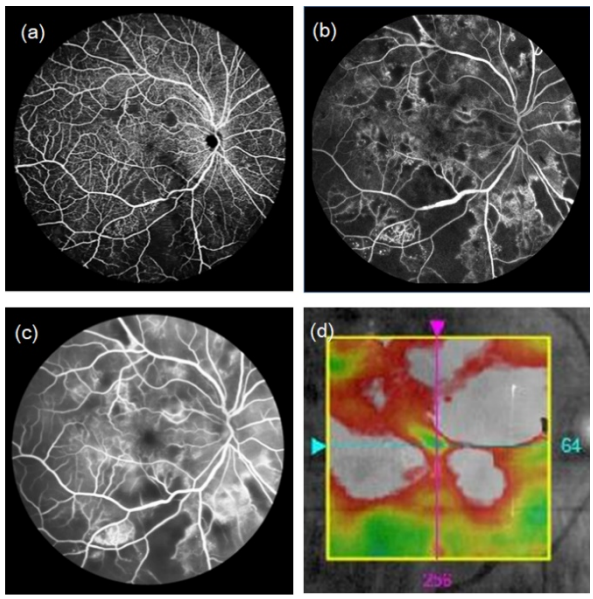

Fig. 3. AI-inferred FA based on OCT-A in diabetic retinopathy. (a) The OCT-A serving as the image source, (b) The real FA, (c) AI-inferred-FA, (d) OCT thickness map showing thickened retina caused by leakage.

3.2. Quantitative analysis

For evaluation of the current CNN algorithm, the SSIMs between the AI-inferred FA images and corresponding FA images were calculated. The average SSIM of them was 0.91 ± 0.08 (standard deviation). For example, a small characteristic leakage shown in Fig. 4(a) was accurately regenerated in an AI-inferred-FA image as shown in Fig. 4(b) which cannot be detected in OCT-A as shown in Fig. 4(c). As in this example, the high SSIM score was achieved because the AI-inferred FA images are closely similar to the real FAs. The SSIM measured between OCT-A and aligned FA was 0.073 ± 0.0039. The average Peak Signal-to-Noise Ratio (PSNR) value between FA and AI-FA was 26.71 ± 2.12 (standard deviation).

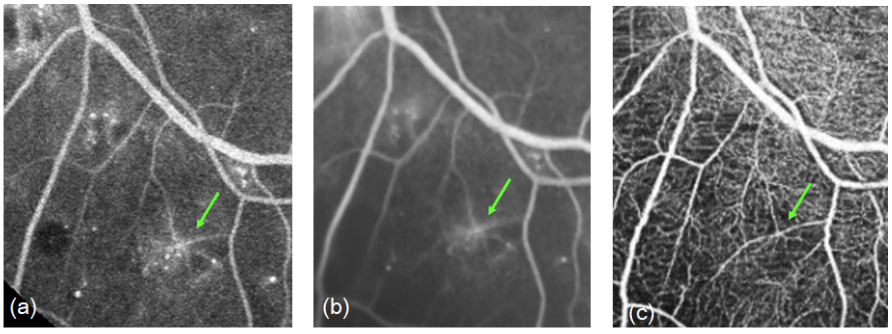

Fig. 4. Excellent reproduction of fine leakage. (a) The arrow indicates fine vascular leakage in real FA, (b) AI-inferred-FA accurately reproduced this fine leakage (arrow), (c) In the OCT-A source image, this fine leakage cannot be detected by the human eye (arrow). Some microaneurysms that cannot be detected in OCT-A (c) are delineated in AI-inferred-FA (b) since they are associated with leakage.

Biomedical Optics EXPRESS

3.3. AI-inferred FA based on OCT-A in BRVO

To investigate the eligibility of the current CNN algorithm for AI-inferred-FA which had been trained using diabetic retinopathy, AI-inferred-FA was generated from OCT-A of BRVO. BRVO, like diabetic retinopathy, belongs to the category of retinal vascular occlusive disorders. In these conditions, vascular leakage is caused by the ischemia-induced VEGF. OCT-A clearly delineated wide-spread non-perfusion areas in the upper half of the fundus image but no leakage as shown in Fig. 5(a). Conventional real FA showed both non-perfusion areas and associated leakage, as shown in Fig. 5(b). AI-inferred-FA showed a closely similar image that depicts both non-perfusion areas and leakage shown in Fig. 5(c). However, what is interesting is the fact that the leakage from obstructed large veins is not fully illustrated in this AI-inferred-FA of BRVO in Fig. 5(b), probably because obstruction of large veins is not a characteristic of diabetic retinopathy. The current CNN algorithm was developed using FA images of diabetic retinopathy as training data.

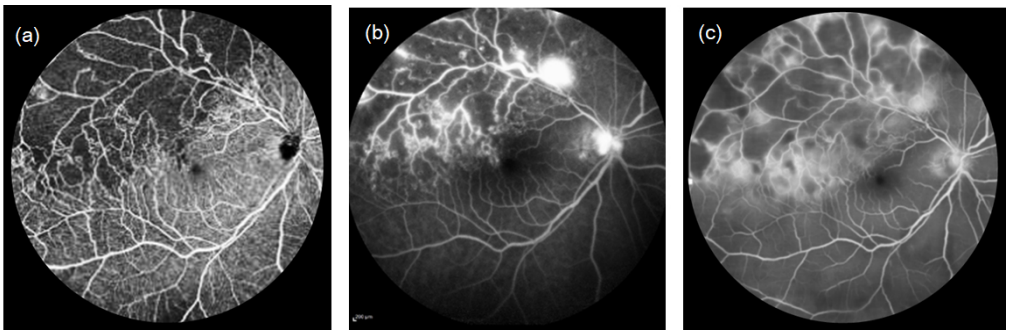

Fig. 5. AI-inferred FA based on OCT-A in diabetic retinopathy. (a) The OCT-A source image, (b) Real FA delineating leakage (c) AI-inferred-FA clearly reproduce retinal vessels and their leakage, which increased over time.

3.4. AI-inferred FA based on OCT-A in Bechet's disease

OCT-A of Behcet's disease looked largely normal without vascular occlusion. Conventional FA of the same eye demonstrated the characteristic fern-like leakage pattern associated with Behcet's disease, which is caused by vascular inflammation but not ischemia. AI-inferred-FA failed to reproduce the fern-like leakage and was evaluated as non-diagnostic.

3.5. AI-inferred FA at various elapsed time points

This CNN algorithm can generate AI-inferred-FA images at any desired elapsed time by inputting tensor data generated by concatenating scalar values indicating image acquisition times and the pixel values of OCT-A image data. This capability is critical for using AI-inferred-FA in actual clinical practice since leakage patterns change with time in real FA, and this information is essential to make a precise diagnosis and treatment plan. Based on a single OCT-A demonstrated in Fig. 5 (a), AI-inferred-FA images were generated corresponding to various elapsed times, at 80 seconds as demonstrated in Fig. 6(a), at 180 seconds as demonstrated in Fig. 6(b), and at 300 seconds as demonstrated in Fig. 6 (c). The leakage increased with elapsed time, just as it does in real FA.

This functionality allows for the creation of AI-inferred-FA videos. One hundred and fifty still AI-inferred-FA images, corresponding to three hundred seconds of real-time, were generated using the aforementioned CNN algorithm. These images were then concatenated to generate a 15-second FA video in eyes with BRVO and diabetic retinopathy, successfully reproducing

Biomedical Optics EXPRESS

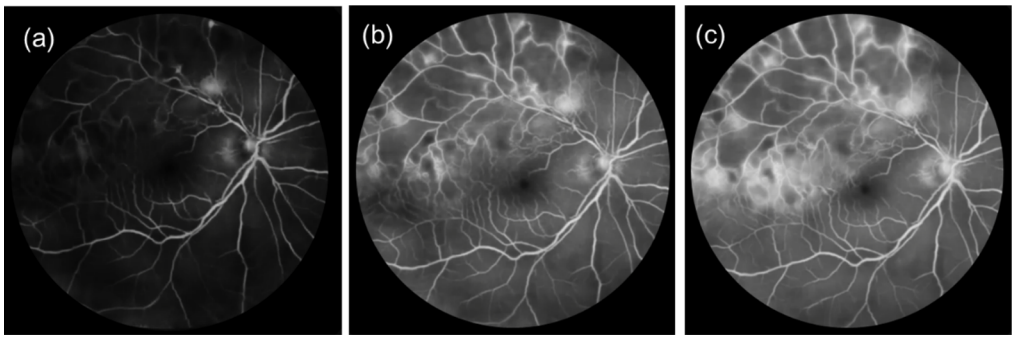

Fig. 6. AI-inferred FA at various elapsed times. (a) at 80 seconds, (b) at 180 seconds (c) at 300 seconds. AI-inferred-FA reproduces the increase in leakage observed over time in real FA.

AI-inferred-FA videos. The AI-inferred-FA video closely resembled the real FA video that shows widespread capillary nonperfusion and gradually increasing leakage at the border of perfused and nonperfused retina, where microaneurysms and dilated vessels are formed.

4. Discussion

Deep learning methods have been successful in improving OCT-A utility in retinal imaging, where most efforts are focused on the segmentation and classification tasks [29–31]. Here, we designed a CNN-based U-Net type [23,24] encoder and decoder modules for biomedical image segmentation to generate AI-inferred-FA using OCT-A as the source images. OCT-A delineates defined retinal vessel images to capillary levels and provides information on capillary non-perfusion areas or neovascularization as shown in Fig. 3(a). OCT-A is a recently introduced imaging technology and has already been widely accepted among ophthalmologists for assessing ocular circulation because the images closely resemble those of conventional real FA, a golden-standard of retinal circulation evaluation method. In FA, blood flow is subjectively categorized as either perfused or non-perfused areas as shown in Fig. 3(b). Perfusion status can be numerically quantified through the utilization of OCT-A, given its visualization of vessels extending up to capillary levels [32,33]. One and probably the only drawback of OCT-A is its inability to depict leakage, which is typically visualized through the presence of extravasated fluorescein dye in conventional FA. OCT-A, which does not require intravenous fluorescein dye, offers the added advantage of enhanced safety by eliminating the risk of anaphylactic shock. However, the trade-off is that this absence of contrast dye usage in OCT-A prevents the detection of vascular leakage phenomena.

In the current study, AI-inferred-FA images successfully and clearly delineated leakage as shown in Fig. 3(c), correctly corresponding to the areas of macular edema depicted as red/white-colored lesions with an OCT thickness map as shown in Fig. 3(d). Thus, we can acquire all necessary information about retinal circulation and resulting macular edema by utilizing OCT-A with AI-inferred-FA at levels equivalent to conventional golden-standard FA, even with reduced image acquisition time and adverse events.

The structural similarity index (SSIM) between the AI-inferred FA images and corresponding conventional FA images was 0.91 ± 0.08. This result demonstrates the high morphological reproducibility of the current CNN algorithm. For instance, a small leakage with a characteristic shape observed in conventional FA shown in Fig. 4(a) was accurately replicated in the AI-inferred-FA images illustrated in Fig. 4(b), a feature that was undetectable in OCT-A shown in Fig. 4(c) to the human eye.

We evaluated the applicability of the current CNN algorithm, trained using actual FA images of diabetic retinopathy, to two other conditions: BRVO and Behcet's disease. BRVO exhibits

Biomedical Optics EXPRESS

vascular leakage through mechanisms akin to those of diabetic retinopathy, involving ischemia-induced VEGF in non-perfusion areas of the retina. On the other hand, the distinctive fern-like leakage observed in Behcet's disease arises from vascular inflammation.

In BRVO, OCT-A clearly delineated non-perfusion areas in the half of the fundus image, but no leakage was shown in Fig. 5(a), while conventional real FA depicted both non-perfusion areas and associated leakage shown in Fig. 5(b). AI-inferred-FA showed a closely similar image to conventional FA that depicted both non-perfusion areas and leakage as shown in Fig. 5(c). On the contrary, AI-inferred-FA based on the corresponding OCT-A of Bechet's disease did not delineate the distinctive fern-like leakage characteristic of Bechet's disease and was evaluated as non-diagnostic.

It is important to note that the vascular leakage observed in uveitis, including Behcet's disease, is primarily attributed to inflammatory processes rather than the upregulation of VEGF resulting from retinal ischemia, which is observed in diabetic retinopathy, utilized as training data, and BRVO. These data suggested that the current CNN algorithm is applicable only for leakage detection in retinal vascular occlusive diseases but not in retinal inflammatory diseases.

The degree of vascular leakage intensifies over time in conventional FA. Therefore, it is essential to incorporate the elapsed time since the injection of contrast dye when generating AI-inferred FA images based on single OCT-A image. The current CNN algorithm was trained by a total of 19,648 FA still images of diabetic retinopathy at various time points after dye injections. One hundred and fifty still FA images corresponding to three hundred seconds of real-time generated using the aforementioned CNN algorithm were concatenated to generate a 15-second FA video in diabetic retinopathy and BRVO. It closely resembled a real FA video that shows widespread capillary nonperfusion and gradually increasing leakage at the border of perfused and non-perfused retina where microaneurysms and dilated vessels are formed.

5. Conclusion

The proposed CNN algorithm aims to provide adjunctive information in OCT-A, specifically leakage patterns, in situations where FA imaging is not feasible in the most and secondary common retinal vascular occlusive disease, i.e., diabetic retinopathy and retinal vein occlusion. While this algorithm is still unable to depict inflammatory leakage, this research serves as a proof-of-concept, demonstrating the potential of artificial intelligence to perform image domain transformation between different imaging modalities like OCT-A and FA. To enhance the effectiveness of our current CNN algorithm, further investigations are warranted using a more expanded repository of OCT-A and FA images encompassing more various diseases. The broader dataset holds the promise of refining the accuracy and robustness of the current CNN algorithm for AI-inferred-FA. This reinforcement could strengthen its diagnostic capabilities and aid in treatment planning.

Acknowledgments. A part of this study was presented during ARVO Annual Meeting 2023.

Disclosures. HIDEAKI MIZOBE, SHUHEI TOBA, are employee of Canon Inc. that produces Canon Xephilio OCT-S1 which was used in this study.

Data availability. Data underlying the results presented in this paper are not publicly available at this time but may be obtained from the authors upon reasonable request.

References

1. A. H. Kashani, C. L. Chen, and J. K. Gahm, *et al.*, "Optical coherence tomography angiography: A comprehensive review of current methods and clinical applications," Prog. Retinal Eye Res. **60**, 66–100 (2017).
2. C. L. Chen and R. K. Wang, "Optical coherence tomography based angiography [Invited]," Biomed. Opt. Express **8**(2), 1056–1082 (2017).
3. E. A. Novais, L. Roisman, and P. R. de Oliveira, *et al.*, "Optical coherence tomography angiography of chorioretinal diseases," Ophthalmic. Surg. Lasers Imaging Retina **47**(9), 848–861 (2016).
4. T. Hirano, K. Hoshiyama, and Y. Takahashi, *et al.*, "Wide-field swept-source OCT angiography (23 × 20 mm) for detecting retinal neovascularization in eyes with proliferative diabetic retinopathy," Graefe's Arch. Clin. Exp. Ophthalmol. **261**(2), 339–344 (2023).

Biomedical Optics EXPRESS

5. C. W. Merkle, M. Augustin, and D. J. Harper, *et al.*, "High-resolution, depth-resolved vascular leakage measurements using contrast-enhanced, correlation-gated optical coherence tomography in mice," Biomed. Opt. Express **12**(4), 1774–1791 (2021).
6. S. Y. Lartey and A. K. Aikins, "Visual impairment amongst adult diabetics attending a tertiary outpatient clinic," Ghana Med. J. **52**(2), 84–87 (2017).
7. A. Arabi, R. Tadayoni, and H. Ahmadieh, *et al.*, "Update on management of non-proliferative diabetic retinopathy without diabetic macular edema; is there a paradigm shift?" J. Ophthalmic Vision Res. **17**, 108–117 (2022).
8. T. Murata, T. Ishibashi, and A. Khalil, *et al.*, "Vascular endothelial growth factor plays a role in hyperpermeability of diabetic retinal vessels," Ophthalmic Res. **27**(1), 48–52 (1995).
9. S. Cai and N. M. Bressler, "Aflibercept, bevacizumab or ranibizumab for diabetic macular oedema: recent clinically relevant findings from DRCR.net Protocol T," Curr. Opin. Ophthalmol. **28**(6), 636–643 (2017).
10. R. Kawasaki, M. Bauer, and V. Bezlyak, *et al.*, "Treatment patterns for retinal diseases in patients newly-treated with anti-VEGF agents: A retrospective analysis of claims data from the Japan Medical Data Center database," Jpn. J. Ophthalmol. **65**(2), 215–226 (2021).
11. P. Romero-Aroca, J. Reyes-Torres, and M. Baget-Bernaldiz, *et al.*, "Laser treatment for diabetic macular edema in the 21st century," Curr. Diabetes Rev. **10**(2), 100–112 (2014).
12. F. Reeser, J. Fleischman, and G. A. Williams, *et al.*, "Efficacy of argon laser photocoagulation in the treatment of circinate diabetic retinopathy," Am. J. Ophthalmol. **92**(6), 762–767 (1981).
13. E. C. Jorge, E. N. Jorge, and M. Botelho, *et al.*, "Monotherapy laser photocoagulation for diabetic macular oedema," Cochrane Database Syst. Rev. **2018**(10), CD010859 (2018).
14. T. Hirano, Y. Toriyama, and Y. Iesato, *et al.*, "Effect of leaking perifoveal microaneurysms on resolution of diabetic macular edema treated by combination therapy using anti-vascular endothelial growth factor and short pulse focal/grid laser photocoagulation," Jpn. J. Ophthalmol. **61**(1), 51–60 (2017).
15. T. Hirano, Y. Toriyama, and Y. Iesato, *et al.*, "Effect of leaking foveal microaneurysms on the treatment of center-involving diabetic macular edema: a pilot study," Ophthalmic Res. **61**(1), 10–18 (2019).
16. Y. Takamura, Y. Yamada, and M. Inatani, "Role of microaneurysms in the pathogenesis and therapy of diabetic macular edema: a descriptive review," Medicina (Kaunas) **59**(3), 435 (2023).
17. Y. Fukuda, S. Nakao, and Y. Kaizu, *et al.*, "Morphology and fluorescein leakage in diabetic retinal microaneurysms: a study using multiple en face OCT angiography image averaging," Graefe's Arch. Clin. Exp. Ophthalmol. **260**(11), 3517–3523 (2022).
18. S. Nakao, S. Yoshida, and Y. Kaizu, *et al.*, "Microaneurysm detection in diabetic retinopathy using OCT angiography may depend on intramicroaneurysmal turbulence," Ophthalmol. Retina **2**(11), 1171–1173 (2018).
19. T. E. de Carlo, S. Zahid, and K. J. Bohm, *et al.*, "Simulating vascular leakage on optical coherence tomography angiography using an overlay technique with corresponding thickness maps," Br. J. Ophthalmol. **104**(4), 514–517 (2020).
20. C. Murata, Y. Murakami, and T. Fukui, *et al.*, "Serous Retinal detachment without leakage on fluorescein/indocyanine angiography in MEK inhibitor-associated retinopathy," Case Rep. Ophthalmol. **13**(2), 542–549 (2022).
21. A. Tavakkoli, S. A. Kamran, and K. F. Hossain, *et al.*, "A novel deep learning conditional generative adversarial network for producing angiography images from retinal fundus photographs," Sci. Rep. **10**(1), 21580 (2020).
22. M. F. Beg, M. I. Miller, and A. Trouve, *et al.*, "Computing large deformation metric mappings via geodesic flows of diffeomorphisms," Int J. Comput. Vision **61**(2), 139–157 (2005).
23. X. X. Yin, L. Sun, and Y. Fu, *et al.*, "U-Net-based medical image segmentation," J. Healthc. Eng. **2022**, 1–16 (2022).
24. O. Ronneberger, P. Fischer, and T. Brox, "U-Net: Convolutional Networks for Biomedical Image Segmentation," in *Medical Image Computing and Computer-Assisted Intervention–MICCAI 2015* (Springer International Publishing, 2015), pp. 234–241.
25. J. Kiefer and J. Wolfwitz, "Stochastic estimation of the maximum of a regression function," Ann. Math. Stat. **23**(3), 462–466 (1952).
26. L. N. Smith, "Cyclical learning rates for training neural networks," *IEEE Winter Conference on Applications of Computer Vision (WACV)*, 464–472 (2017).
27. Z. Wang, A. C. Bovik, and H. R. Sheikh, *et al.*, "image quality assessment: from error visibility to structural SiImage quality assessment: from error visibility to structural similarity," IEEE Trans. on Image Process. **13**(4), 600–612 (2004).
28. M. Khayat, M. Williams, and N. Lois, "Ischemic retinal vein occlusion: characterizing the more severe spectrum of retinal vein occlusion," Surv. Ophthalmol. **63**(6), 816–850 (2018).
29. Y. Guo, T. T. Hormel, and S. Pi, *et al.*, "An end-to-end network for segmenting the vasculature of three retinal capillary plexuses from OCT angiographic volumes," Biomed. Opt. Express **12**(8), 4889–4900 (2021).
30. M. Abtahi, D. Le, and J. I. Lim, *et al.*, "MF-AV-Net: an open-source deep learning network with multimodal fusion options for artery-vein segmentation in OCT angiography," Biomed. Opt. Express **13**(9), 4870–4888 (2022).
31. D. L. B. Ebrahimi, M. Abtahi, and A. Dadzie, *et al.*, "Optimizing OCTA layer fusion option for deep learning classification of diabetic retinopathy," Biomed. Opt. **14**(9), 4713–4724 (2023).
32. T. Hirano, J. Kitahara, and Y. Toriyama, *et al.*, "Quantifying vascular density and morphology using different swept-source optical coherence tomography angiographic scan patterns in diabetic retinopathy," Br. J. Ophthalmol. **103**(2), 216–221 (2019).
33. T. Hirano, K. Chanwimol, and J. Weichsel, *et al.*, "Distinct retinal capillary plexuses in normal eyes as observed in optical coherence tomography angiography axial profile analysis," Sci. Rep. **8**(1), 9380 (2018).